

# The Influence of Nutrients Diffusion on a Metabolism-driven Model of a Multi-cellular System

**Davide Maspero\***, **Chiara Damiani<sup>†</sup>**,  
**Marco Antoniotti,<sup>‡</sup>** **Alex Graudenzi<sup>§</sup>**  
*Department of Informatics Systems  
and Communication  
Univ. of Milano-Bicocca, Milan, Italy*

**Giulio Caravagna**  
*Data Scientist  
Institute of Cancer Research  
ICR, London, UK*

**Daniele Ramazzotti**  
*Department of Pathology  
Stanford University  
Stanford, CA 94305, USA*

**Marzia Di Filippo, Marco Vanoni<sup>£</sup>**  
*Department of Biotechnology  
and Biosciences  
Univ. Milano-Bicocca, Milan, Italy*

**Riccardo Colombo**  
*Department of Biomedical  
and Clinical Sciences "L. Sacco"  
Univ. of Milan, Milan, Italy*

**Dario Pescini<sup>C</sup>**  
*Department of Statistics and Quantitative Methods  
Univ. of Milano-Bicocca, Milan, Italy  
dario.pescini@unimib.it*

---

**Abstract.** The metabolic processes related to the synthesis of the molecules needed for a new round of cell division underlie the complex behaviour of cell populations in multi-cellular systems, such as tissues and organs, whereas their deregulation can lead to pathological states, such as cancer. Even within genetically homogeneous populations, complex dynamics, such as population oscillations or the emergence of specific metabolic and/or proliferative patterns, may arise, and this aspect is highly amplified in systems characterized by extreme heterogeneity.

---

\* Also affiliated at: Fondazione IRCCS Istituto Nazionale dei Tumori, Milan, Italy

<sup>†</sup> Also affiliated at: SYSBIO Centre of Systems Biology, Univ. of Milano-Bicocca, Milan, Italy

<sup>‡</sup> Also affiliated at: NeuroMI Milan Center for Neuroscience, Univ. of Milano-Bicocca, Milan, Italy

<sup>§</sup> Also affiliated at: Institute of Molecular Bioimaging and Physiology, Italian National Research Council, Milan, Italy.

<sup>£</sup> Also affiliated at: SYSBIO Centre of Systems Biology, Univ. of Milano-Bicocca, Milan, Italy.

<sup>C</sup> Address for correspondence: Department of Statistics and Quantitative Methods, University of Milano-Bicocca, Via Bicocca degli Arcimboldi, 8 - 20126 Milan.

To investigate the conditions and mechanisms that link metabolic processes to cell population dynamics, we here employ a previously introduced multi-scale model of multi-cellular system, named FBCA (Flux Balance Analysis with Cellular Automata), which couples biomass accumulation, simulated via Flux Balance Analysis of a metabolic network, with the simulation of population and spatial dynamics via Cellular Potts Models.

In this work, we investigate the influence that different modes of nutrients diffusion within the system may have on the emerging behaviour of cell populations. In our model, metabolic communication among cells is allowed by letting secreted metabolites to diffuse over the lattice, in addition to diffusion of nutrients from given sources. The inclusion of the diffusion processes in the model proved its effectiveness in characterizing plausible biological scenarios.

**Keywords:** Multi-scale modeling, Cellular Potts Model, Flux Balance Analysis, Diffusion, Cancer development

## 1. Introduction

Increasing experimental evidences are suggesting that the deregulation of metabolism is one of the key actors in tumor origination and development [1, 2]. In this respect, most current computational strategies to investigate metabolic deregulation are based on the simulation of the steady state behavior of an average cell belonging to a (heterogeneous) population [3, 4].

Yet, cancer (sub)population evolve and compete in a (micro)environment with usually limited resource (e.g., oxygen and nutrients) and with specific spatial properties, which significantly differs in distinct tissues and organs [5]. For this reason, properties based on average measurements may be scarcely significant, as they are not representative of the specific features of single cells and subpopulations, as well as of their interactions with the surrounding environment [6].

This aspect has important translational repercussions, as the intra-tumor heterogeneity resulting from such complex interplay is one of the major causes of drug resistance, therapy failure and relapse [7, 8, 9]. Unfortunately, so far the emerging single-cell omics technologies are still unable to finely characterize the interactions among cell (sub)populations, especially because of many technical issues that compromise the overall resolution [10, 11].

For this reason, effective computational multi-scale models are increasingly needed to account for processes and phenomena occurring at different time/ space scales and involving populations of interacting cells, with the final goal of identifying the conditions that may lead to complex behaviours, such as tissue patterning, cellular migration, homeostasis, and the emergence of pathological states [12, 13]. In this respect, many attempts have been proposed to simulate the spatial/morphological dynamics of multi-cellular systems, by employing biophysically plausible models of cells and their interactions, e.g., within tissues and organs [14, 15, 16]. In general, investigating the emerging spatio-temporal behaviour of the heterogeneous populations may facilitate the development of more effective intervention strategies [17].

In [18], we developed FBCA (Flux Balance with Cellular Automata) as first attempt to connect the dynamical behavior of metabolic networks to biophysically realistic spatial and morphological properties of real multi-cellular systems. This model combines a spatial/morphological dynamical model of a general tissue, simulated via Cellular Potts Model (CPM) [19, 20, 21, 22], and a lower-level model of the metabolic activity of its constituting single cells, computed via Flux Balance Analysis (FBA) [3].

In [23], we extended the previous framework by adding a population density-sensing mechanism, that led to more realistic results.

In this work, we further extended the methodology to model metabolites diffusion through space. In particular, we modeled metabolic communication among cells by allowing metabolites (e.g., lactate secreted by cells) to diffuse over the tissue according to a local spatial gradient. The final goal of this study is to evaluate the impact of different models of nutrient diffusion on the overall cell population dynamics.

## 2. Methods

In order to model a generic multi-cellular system, such as a cell culture or a tissue, we adopted FBCA, which we previously introduced in [18, 23]. This computational methodology combines through a multi-scale model the spatial dynamics representation of the system via CPM [24], with a model of cell metabolism via FBA [3] (see Figure 1).

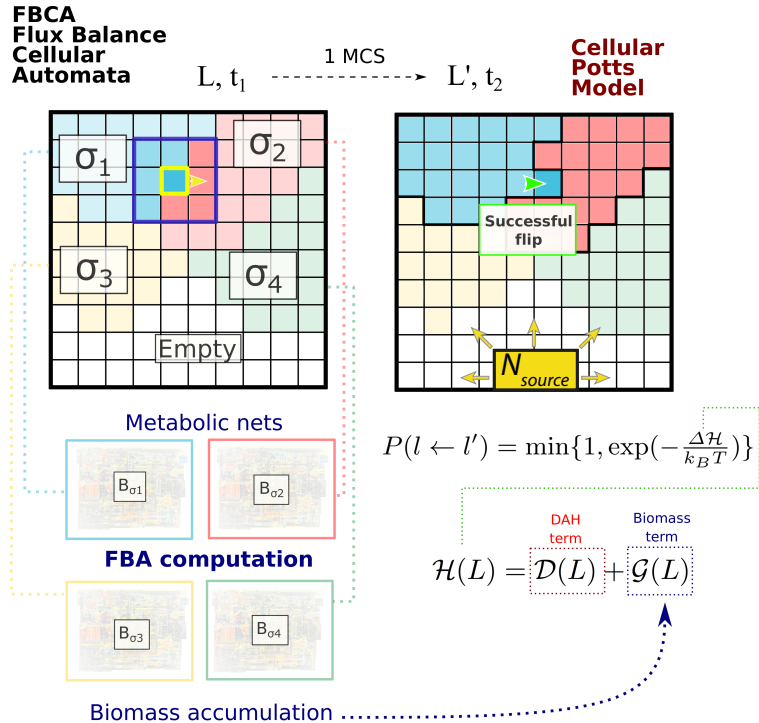


Figure 1. FBCA model is depicted. Image modified from [18]. The morphology of a generic tissue is modeled via Cellular Potts Model, in which biological cells are represented by sets of contiguous lattice sites, which evolve via flip attempts driven by a Hamiltonian function  $\mathcal{H}(L)$ .  $\mathcal{H}(L)$  depends on two terms, the first accounting for the Differential Adhesion Hypothesis (DAH), the second for the growth tendency of each cell due to the accumulation of biomass (see Methods). Biomass is computed via Flux Balance Analysis on cell-specific metabolic networks. Nutrients  $N$  are diffused, from different sources, to sustain the cellular growth.

## 2.1. Simulation approach

According to CPM representation of multi-cellular system, biological cells are represented on a two dimensional lattice  $L$ , and their spatial dynamics is driven by an energy minimization criterion ruled by a Hamiltonian function  $\mathcal{H}(L)$ . A rectangular and rigid grid composed of  $h \times w$  square sites  $l^i \in L$  is used to represent the lattice. Given a set of cells tags  $\mathcal{C} = \{c_c\}$  represented in the lattice  $L$ , where  $c_c \in \mathbb{N}$ , and a set of cellular types  $\mathcal{T} = \{t_t\}$ , where  $t_t \in \mathbb{N}$ , each biological cell is identified through the identifier  $c_c$  and associated to a specific cellular type  $t_t$ . The space occupied by cell  $c_c$  on the lattice is denoted as  $C_c \subseteq L$  and corresponds to the set of contiguous lattice sites  $l^i$  associated to cell  $c_c$ . It is possible to represent on the lattice the empty space assigning to a lattice site the cellular type  $E$  (or the empty space).

To connect the information of lattice sites with the information of cells, it is possible to exploit  $[N(l^i)]$ , that is the concentration for a nutrient  $N$  at a specific lattice site  $l^i$ , together with the definition of two operators:

- $\sigma : L \rightarrow \mathcal{C}$  such that  $\sigma(l^i) = c_c$ . For short, we can say that  $\sigma_i = c$ , where  $c$  is the identifier of the cell that lies on lattice site  $l^i$ .
- $\tau : \mathcal{C} \rightarrow \mathcal{T}$  such that  $\tau(\sigma_i) = \tau(\sigma(l^i)) = t_t$ . For short, we can say that  $\tau_i = t$ , where  $t$  is the cellular type that is associated to the cell that lies on lattice site  $l^i$ .

### The simulation

The simulation approach can be depicted as follows:

1. Initialize:  $L, \mathcal{C}, N$
2. For each simulation step:
  - FBA computation
  - Biomass accumulation
  - Removal of cell death by lacking of nutrient
  - Minimization of the Hamiltonian function
  - Cell cycle phase evaluation
  - Nutrient diffusion

Each step of the second phase is detailed in the following.

*FBA computation.* FBA is exploited to compute the biomass production rate of any cell present in the lattice according to the corresponding nutrient availability. To this aim, a metabolic network model of human central carbon metabolism consisting of 272 reactions and 240 metabolites is associated to each cell  $c_c$ ; this model was introduced in [25]. A metabolic network is defined as the set of metabolites and chemical reactions taking place in a cell, and it can be formalized as a  $M \times R$  stoichiometric matrix  $S$ , where  $M$  is the number of metabolites and  $R$  is the number of reactions. Each element  $s_{m,r}$  of the matrix  $S$  is the stoichiometric coefficient of metabolite  $m$  in reaction  $r$ , which expresses the number

of molecules of metabolite  $m$  that are transformed in reaction  $r$ . For any cell, uptake rate boundaries of extracellular nutrients are defined according to the simulated experimental setting. In general, the uptake rate of a given metabolite is constrained to be lower than the sum of the corresponding concentration values in all of the lattice sites in that cell closeness. For the sake of simulation, flux values of extracellular nutrients uptake reactions are assumed to be proportional to the concentration of the corresponding involved nutrient.

Given a metabolic network, Linear Programming is applied in FBA simulations to identify the flux distribution  $\mathbf{v} = (v_1, \dots, v_R)$  that maximizes or minimizes a specific objective function  $Z$ :

$$Z = \sum_{j=1}^R w_j v_j \quad (1)$$

where  $w_j$  is a coefficient that represents the contribution of flux  $v_j$  in vector  $\mathbf{v}$  to  $Z$ , given a steady-state assumption for the abundance of each metabolite, i.e.,  $S \mathbf{v} = \mathbf{0}$ . In this work, the Linear Programming Problem is solved at each *Monte-Carlo Step* (MCS) to maximize for each cell a pseudo-reaction that represents the conversion rate of biomass precursors into biomass, as follows:

$$\begin{aligned} & \text{maximize } v_b \\ & \text{subject to } S \mathbf{v} = \mathbf{0}, \mathbf{v}_L \leq \mathbf{v} \leq \mathbf{v}_U \end{aligned} \quad (2)$$

where  $v_b$  is the biomass reaction flux of the cell  $c_c$ , whereas  $\mathbf{v}_L$  and  $\mathbf{v}_U$  represent the vectors containing, respectively, minimum and maximum allowed reaction fluxes.

*Biomass accumulation.* At each time step  $s$ , the current value of the biomass so far accumulated by a given cell  $c_c$  is represented by the map  $\mathcal{B} : \mathbb{R} \times \text{time} \rightarrow \mathbb{R}$ , that is  $\mathcal{B}(\sigma_i, s) = \mathcal{B}(c, s)$ . To update the current value for  $\mathcal{B}(c, s)$ , we add the biomass synthesis rate  $v_b$  obtained from the FBA simulation for the corresponding cell, to the biomass that is so far accumulated by the cell itself:

$$\mathcal{B}(c, s) = \mathcal{B}(c, s - 1) + \gamma \cdot v_b \quad (3)$$

where  $\gamma$  is a dimensionless factor linking the contribution of cell density to biomass accumulation.  $\mathcal{B}(c, s)$  is exploited to determine the corresponding *cell density*  $\rho_c = \frac{\mathcal{B}(c, s)}{A_c}$ .

In [18], we considered the scenario where, at each time step, a given cell produces biomass according only to the nutrient availability, disregarding other parameters and setting the factor  $\gamma$  equal to 1 to make the biomass accumulation independent of the current cellular density. However, in a more realistic scenario, proposed in [23], cells avoid an uncontrolled raising of their cell density  $\rho_c$ , we therefore modelled the limitation of biomass accumulation  $\mathcal{B}(c, s)$  at each time step introducing a limiting factor  $\varphi \in \mathbb{R}^+$  as follows:

$$\gamma = \begin{cases} 1, & \text{if } \rho_c \leq \varphi \\ 1 - \min(1, 2(\frac{\rho_c}{\varphi} - 1))^2, & \text{otherwise} \end{cases}$$

In this way, we prevent the increase of the biomass accumulation in case of  $\rho_c$  exceeding its initial value of 1.5 times.

*Hamiltonian function.* The Hamiltonian function  $\mathcal{H}(L) : L \rightarrow \mathbb{R}$ , is composed of two terms  $\mathcal{H}(L) = \mathcal{D}(L) + \mathcal{G}(L)$  that, respectively, account for the Differential Adhesion Hypothesis (DAH)  $\mathcal{D}(L)$  [26], and the growth tendency  $\mathcal{G}(L)$  of each cell that is driven by biomass accumulation:

The first term  $\mathcal{D}(L)$  is defined as follows:

$$\mathcal{D}(L) = \frac{1}{2} \sum_{i,j \in \mathcal{N}} J(\tau_i, \tau_j)(1 - \delta_{\sigma_i, \sigma_j}) \quad (4)$$

where  $J(\tau_i, \tau_j)$  is the surface energy between cellular types  $\tau_i$  and  $\tau_j$  that is required to maintain adjacent two cell sites,  $\delta_{\sigma_i, \sigma_j}$  is the Kronecker delta, and  $\mathcal{N}$  is the Moore neighborhood.

The second term  $\mathcal{G}(L)$  is defined as follows

$$\mathcal{G}(L) = \lambda \sum_{c \in \mathcal{C}} (A_c - A_{\oplus}(\mathcal{B}(c, s)))^2 \quad (5)$$

where the plasticity coefficient  $\lambda \in \mathbb{R}^+$  is a Lagrange multiplier that accounts for the capacity to deform a cell membrane, whereas  $A_c$  is defined as  $A : L \rightarrow \mathbb{N}$  such that  $A(\sigma(l^i)) = A(\sigma_i) = A(c_c) = A_c$  and corresponds to the current area of the cell  $c_c$ . The target area  $A_{\oplus}(\mathcal{B}(c, s))$  is function of the biomass  $\mathcal{B}(c, s)$  that is accumulated by the cell  $c_c$  at each time step according to the current nutrient availability. The latter depends on the adopted diffusion process according to the considered environmental settings, as it will be discussed later in this Section in the paragraph Diffusion. The accumulated biomass  $\mathcal{B}(c, s)$  is converted into the corresponding  $A_{\oplus}$  by using the conversion factor  $\varphi$ ,  $A_{\oplus} = \frac{\mathcal{B}(c, s)}{\varphi}$ , which is usually set to 50.

*Cell cycle phase evaluation.* We associate to each cell an initial equal area, which is called base area  $A_B$ , representing the corresponding initial area before a cell starts to grow. Each cell can grow until it reaches twice the initial  $A_B$ . After that, following the half splitting of the updated space along a randomly chosen horizontal or vertical direction, a daughter cell characterized by cell properties inherited from its parent is produced.

*Diffusion.* The nutrient diffusion process, driven by the resulting positive outcomes shown in [27], is here implemented averaging the nutrient concentrations in a neighborhood  $I$  of each lattice site  $l^i$ :

$$[N(l^i)] = \frac{D}{|I|} \sum_{j \in I} [N(l^j)] \quad (6)$$

where, the neighborhood  $I$  has different definition according to the biological setting to be mimicked, i.e.  $I := \mathcal{N} \cup l^i$  in case of permeable cells, or  $I := C_E \cap (\mathcal{N} \cup l^i)$  in case of impermeable cells.  $C_E$  refers to the lattice sites where nutrients cannot diffuse because they are occupied by impermeable cells.  $D$  is the diffusion coefficient chosen based on the nutrient species.

## 2.2. FBCA and diffusion

To investigate the ability of the proposed approach discussed in Section 2.1 to simulate the impact of diverse nutrient diffusion models on a cell population dynamics, we modelled two different biological scenarios corresponding, respectively, to a closed environment and to a tissue like environment.

Regarding the latter, we proposed two configurations relative to the geometry of the nutrient sources. These two configurations represent, respectively, a cross and a longitudinal section of the tissue like environment (see Figure 2 panels A and B). Finally, to evaluate different descriptions of nutrient diffusion across cellular membranes, namely cell membranes permeability, we modelled both cross and longitudinal section configurations by considering cells as permeable and impermeable.

Overall, all these investigated scenarios share the following properties: i) the lattice is a fully closed environment where the process of cellular death by starving is the only way to remove cells; ii) in [23], the limitation of biomass accumulation allowed to obtain outcomes that are close to the biological reality. For this reason, we maintain the assumption in this work; iii) metabolism of each cell is simulated by using a core model of human central carbon metabolism [25, 28, 29]; iv) in this study we consider one cellular type  $c$  and empty space  $E$  i.e.  $\mathcal{T} = \{c, E\}$ , with surface energies  $J(c, c) = 8$  and  $J(c, E) = 2$ , mimicking the tendency to fill the empty space if available. Finally, simulation parameters are set as in [18], unless otherwise specified.

### 2.2.1. Nutrients distribution and geometry

The first simulated biological scenario corresponds to a closed environment. In this regard, we modelled a rectangular lattice space consisting of  $150 \times 100$  sites. In this configuration, metabolites are uniformly distributed over the lattice and their concentration values are equally set in all the lattice sites. Furthermore, intercellular interactions only depend on nutrients exchange rather than on specific nutrient diffusion dynamics.

In the initialization phase, the lattice is populated with four cells having the same area. At each simulation time step: i) to reset a uniform nutrients distribution over the lattice, the amount of each nutrient at each lattice site,  $[N(l^i)]$  is set to its mean value over the entire lattice; ii) nutrients uptake rate of each cell is set proportionally to its area  $A_c$  and constraints of each cell  $\mathbf{v}_U, \mathbf{v}_L$  are set to  $[N(l^i)] \cdot A_c$ ; iii) a FBA optimization is performed for each and every cell being in the lattice, and the secreted metabolites instantaneously diffuse; iv) finally, the nutrients amount in the lattice is updated. The simulation is halted before that cells saturate the closed environment (i.e. 1000 time steps) according to the biological inspiration.

In the second biological scenario, we conceived a rectangular lattice space of  $175 \times 115$  sites to represent a tissue-like environment. Moreover, this lattice is completely closed to avoid the removal of cells from the system beyond the cell death. According to this space configuration, nutrient diffusion dynamics is considered and metabolites concentration in each lattice site  $[N(l^i)]$  is set equal to the mean of the corresponding concentrations in its neighborhood according to Equation 6. In the initialization phase, the lattice is randomly populated with cells of different initial area.

Many projections are possible sections of a three dimensional space into a two dimensional one, but to pursue our intent to mimic realistic conditions of a tissue, we opted for the following two sections.

*Cross section* represents a transversal section of a generic biological tissue that consists of 5 square nutrient sources that are fixed placed within the lattice. These point sources represent blood vessels from which nutrients radially diffuse. As depicted in Figure 2A, vessels area is equal to 121 lattice sites per the top and bottom point sources, whereas it is equal to 81 for the three central ones.

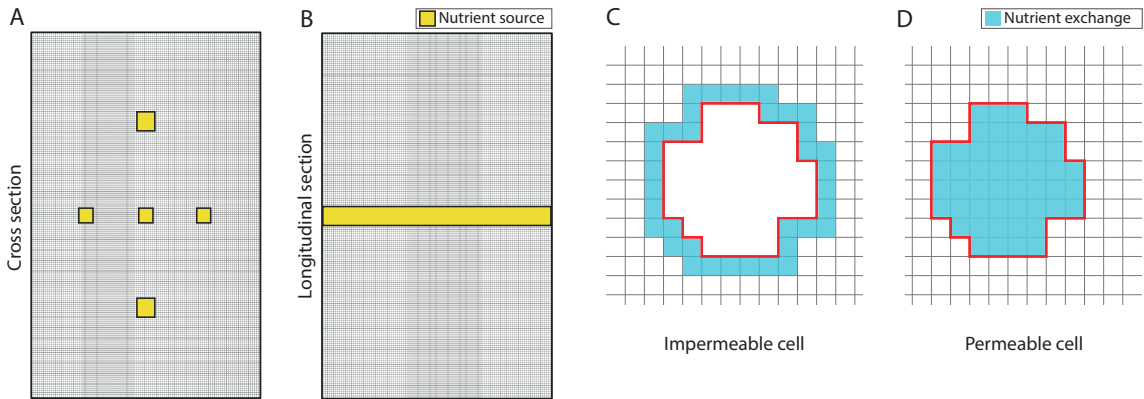


Figure 2. Schematic representation of the nutrient sources geometry and access. On the left: A) The tissue is represented from a cross section point of view. B) The tissue is represented from a longitudinal section point of view. Yellow rectangles and squares show the position and the area of the nutrient sources in the lattice. On the right: Cells have different nutrient availability (light blue surface) according to their permeability. C) Impermeable cells exchange nutrients with lattice sites of the empty space adjacent to cell membrane (red solid lines); D) permeable cells exchange nutrients with lattice sites within the cell membrane.

*Longitudinal section* represents a biological tissue traversed by a blood vessel. The blood vessel is here represented as a rectangle occupying all the central area of the lattice equal to  $11 \times 115$  lattice sites. In this configuration, nutrients diffuse in the lattice with a linear gradient perpendicular to the vessel axis.

The geometry and the position of the nutrient source are the only elements discriminating the two tissue like configurations. At each diffusion step, each one of the considered nutrients concentration within lattice sites of the source area is set equal to a specific value, i.e., oxygen is equal to 100 fmol, glucose is equal to 50 fmol, and glutamine is equal to 50 fmol. The lactate is not supplied in the extracellular environment, but it may be just produced and then exchange from the cells. Once nutrients concentration values are updated in these lattice sites, the diffusion in the entire lattice occurs according to equation 6. If nutrients are not consumed by cells, they are removed from the simulated lattice through a constant flux value when the corresponding edges of the lattice itself are reached.

### 2.2.2. Cell membrane permeability

In this work, we devise a simulator suitable to investigate the interplay between cellular population dynamics and nutrient diffusion. In this framework two different length scales take place: the one of the nutrients that has dimensions of  $\text{\AA}$  and the one of the cells that has length of  $\mu\text{m}$ . This, combined with the fact that we exploit lattices, bi-dimensional objects to represent cells, three-dimensional objects, suggested us to compare two different descriptions of nutrient diffusion across cellular membranes, permeable versus impermeable cells (see Figure 3).

*Permeable cell.* In this condition, cell and nutrients move on two distinct overlapping layers: the cell matrix, in which cells evolve, overlays the nutrient matrix, where metabolites freely diffuse disregarding the presence of the cells. In this configuration, cells have access to the nutrients and

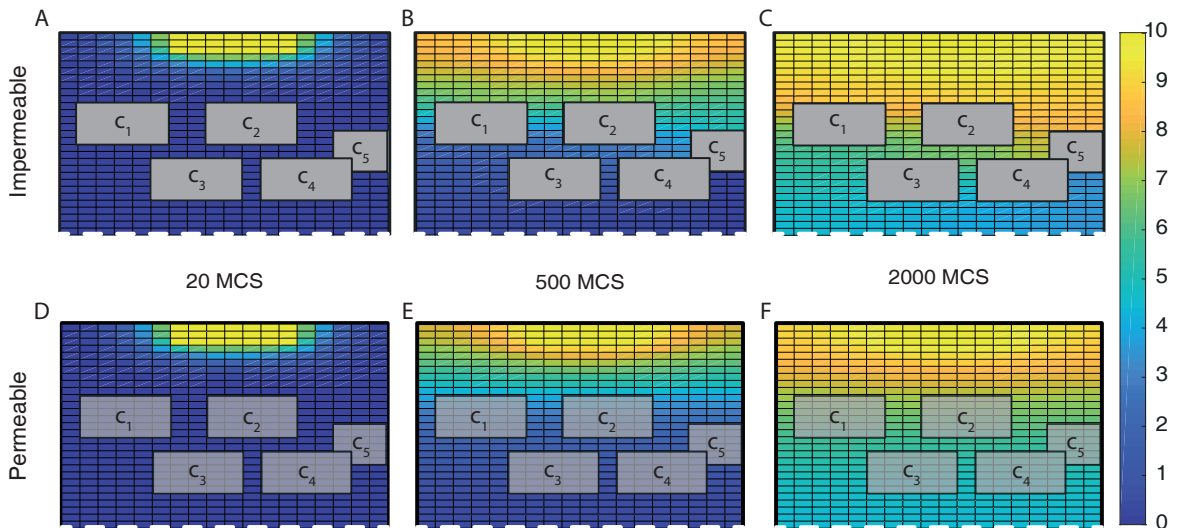


Figure 3. Nutrient diffusion simulation. In each frame the same environment is depicted with a lattice populated with five cells ( $C_1, \dots, C_5$ ) where in each lattice site  $l^i$  the color correspond to the concentration of a generic nutrient  $[N(l^i)]$  at that time step. In this dynamics there is no interaction between cells and nutrient but the space occupied by each cell. Comparing the upper part (impermeable setting) with the lower one (permeable setting), it is possible to recognize the shading effect, due to the cellular membrane, and the slower diffusion process due to the limited amount of space available to nutrients to the impermeable configuration.

metabolites of each lattice site over which they “float” (See Figure 2D). The set of lattice sites in which diffusion takes place  $I = \mathcal{N} \cup l^i$  does not require that sites belong to the empty space. In the same way, the metabolites produced by each cell flow only into those lattice sites under the same cell surface  $C$ . Cells are completely permeable to nutrients and metabolites and the diffusion process takes place “independently” from the cells positions.

*Impermeable cell.* Cells and nutrients share a common layer, and nutrient diffusion is strongly affected by cells locations. In this scenario, cells are fully impermeable to nutrients. Consequently, nutrients cannot diffuse in the lattice sites that are occupied by cells (See Figure 2C). Set  $I = C_E \cap (\mathcal{N} \cup l^i)$  adopted in Equation 6 requires to consider only lattice sites belonging to the empty space. In this configuration, cells only access to metabolites that are available in lattice sites adjacent to their external surface. In a similar manner, the metabolites produced by each cell flow only into lattice sites on the perimeter of the cell surface. However, in this way, two neighbouring cells that are separated by just a unique lattice site, share the set of nutrients in lattice sites that are adjacent to cellular external sides. To avoid the situation where a limiting nutrient concentration is consumed by both cells, we updated the corresponding nutrients concentration values after metabolic fluxes computation of each single cell. Moreover, to avoid bias, we randomized the order in which these optimizations were performed. Since nutrient diffusion and computation of the cellular dynamics are sequentially executed, if cell area increase includes a previously empty lattice site, nutrients concentration is shifted in that lattice site and then splitted among its neighborhood belonging to the set of empty sites.

## 2.3. Implementation

The scripts to perform all the analysis and the functions to simulate the spatial dynamics and the diffusion steps has been written from scratch in Matlab. We used the COBRA Toolbox[30] to optimize the metabolic networks and compute the biomass for each cell in the lattice. A complete MCS requires between  $\sim 3$  s and  $\sim 6$  s with a PC Intel Core i7-3770 CPU 3.40 GHz 64-bit capable, with 32 GB of RAM DDR3 1600 MT/s.

## 3. Results

### 3.1. Closed environment

As shown in Figure 4, when we modelled the closed environment setting, we observed that cells start to grow and to fill the empty available space. Nevertheless, cells dimension does not increases excessively because of the previously defined growth rules with a mitotic area set to 50.

Moreover, Figure 4 contains few snapshots of the metabolic history of the entire cells population suggesting a metabolic switch from glucose uptake to lactate consumption: cells turn from red to blue.

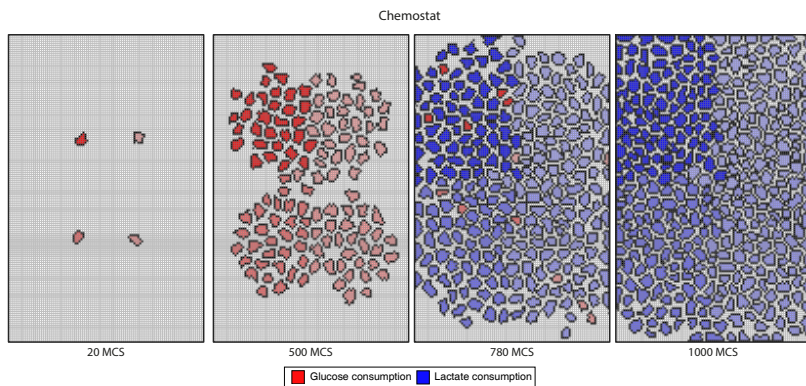


Figure 4. Cells population dynamics in the closed environmental setting. In this configuration, metabolites are uniformly distributed over the lattice and their concentration values are equally set in all the lattice sites. Intercellular interactions only depend on nutrients exchange rather than on a specific nutrient diffusion dynamics. The color assigned to each cell depends on its emerging metabolic trait. Red cells depend on glucose utilization, while the blue ones on lactate utilization. Color shades are intended to distinguish among cells and are not informative about fluxes values.

But, it is in Figure 5 that is possible to account for this phenomenon, at the beginning glucose and glutamine represent the main nutrients adopted from cells to grow, even if the initial consumed concentration of glucose is higher than that of glutamine. Moreover, from the red curve in Figure 5 A, that corresponds to the available amount of glucose over time and space, we observed that cell consumption of this nutrient does not follow a linear trend due to the initial low number of cells that are present in the lattice.

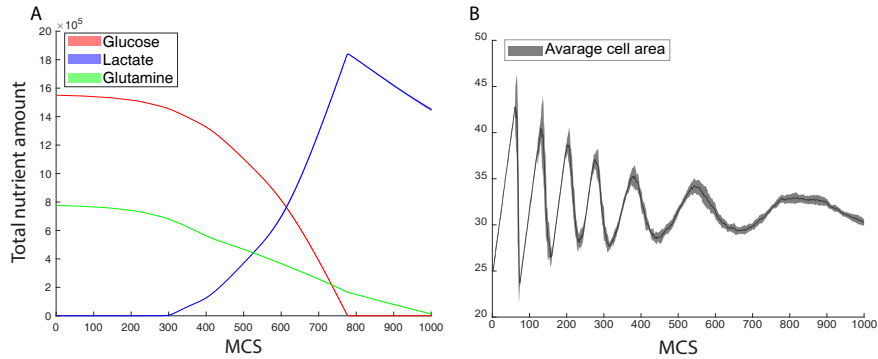


Figure 5. Nutrient dynamics and average area in the closed environment setting. A) The graph depicts the mean nutrients amount (solid line) and its standard deviation (shaded area) over 10 independent simulations. B) The graph depicts the mean cell area (solid line) and its standard deviation (shaded area) over 10 independent simulations.

These two nutrient sources are gradually consumed over MCS time step and lactate is produced. However, at the point where there is no more available glucose to grow, we observed that cells start to use lactate as alternative nutrient source. Accordingly, in the second and third panel of Figure 4, we observed a rapid switch of cellular metabolism from cells mainly growing on glucose to cells whose growth is dependent on the consumption of lactate. This rapid switch can occur because of the identical access of cells to nutrients. In line with the description of closed environment setting, nutrients access only changes among cells according to their dimension.

In Figure 5B, we plotted the average cell area over MCS. The starting setting of 4 cells having the same area showed very well the cellular growth process due to the initial sharp increase of cell average area. Moreover, we can appreciate how long it takes a cell to double, i.e., the mitosis process. As cells continue to grow, we observed that their number increases, and differences begins to emerge among them due to the no longer equal size. Accordingly, the average cell area results to be the mean of a more extended range of values.

### 3.2. Tissue like environment

In the tissue-like model, we consider that all cells can be either permeable or impermeable to nutrients. Our simulations consider either a longitudinal or a cross-section of a 3D lattice, therefore originating 4 independent simulation scenarios (Figure 6).

In all scenarios, nutrients are injected in the system only within a specialized lattice subset that we refer to as “vessel”, they mix only locally and cells can move and die (because of nutrient depletion). Since their survival chances collapses as they move away from nutrient availability, cells tend to stay close to the vessels in all four simulation scenarios over the course of the entire simulation (Figure 7).

Snapshots of the lattices at the end of simulations are shown in Figure 6. We assigned cells in the population to three groups according to their way of metabolizing lactate, taken as an indication of

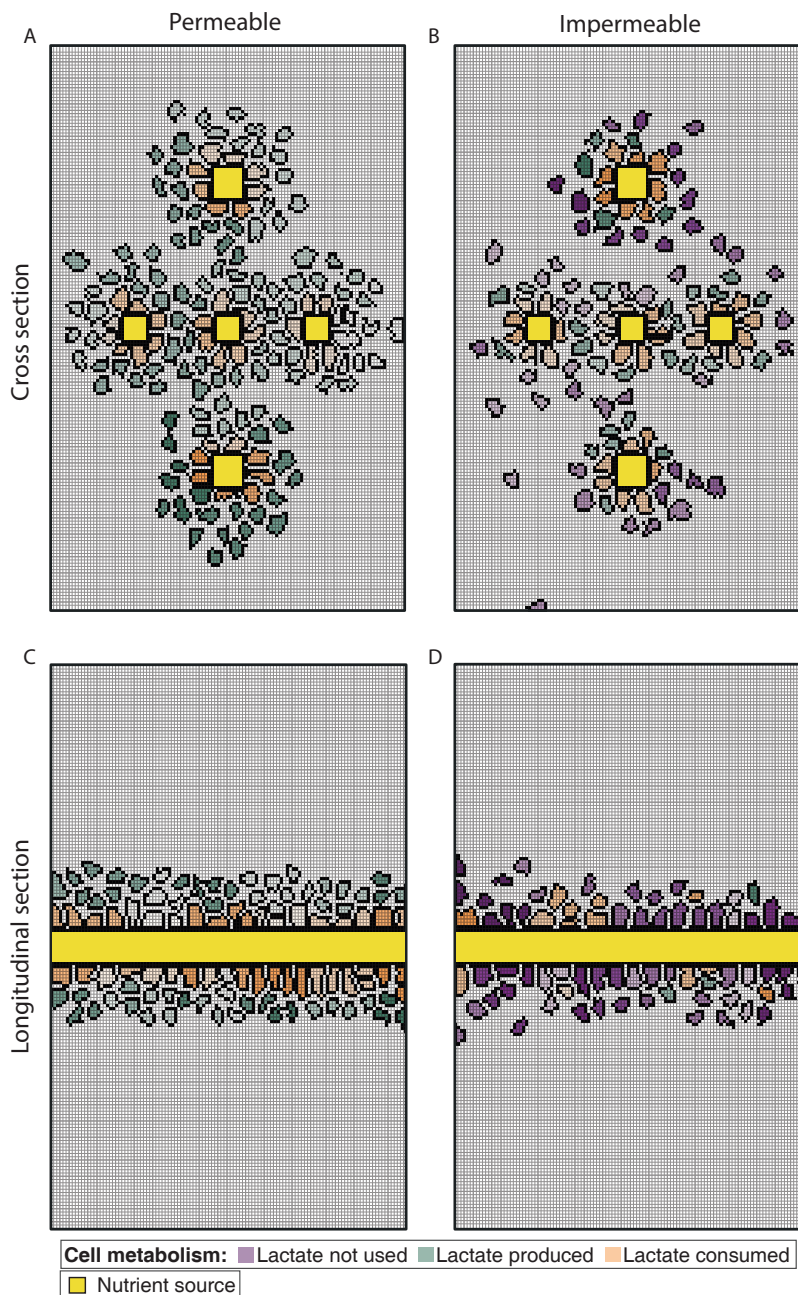


Figure 6. Snapshot of the final simulation step relative to cell population arrangement according to the four possible configurations of tissue environmental setting. The tissue is represented from a cross section (panels A,B) and from a longitudinal section point of view (panels C, D). The cells have permeable membrane (panels A, C) and impermeable membrane (panels B, D). The yellow lattice sites represent the nutrient sources in the lattice. Biological cells are differently colored according the corresponding lactate metabolism, i.e. green if lactate is produced, orange is lactate is consumed and purple if lactate is both produced or consumed with a flux less than 0.1 fmol.

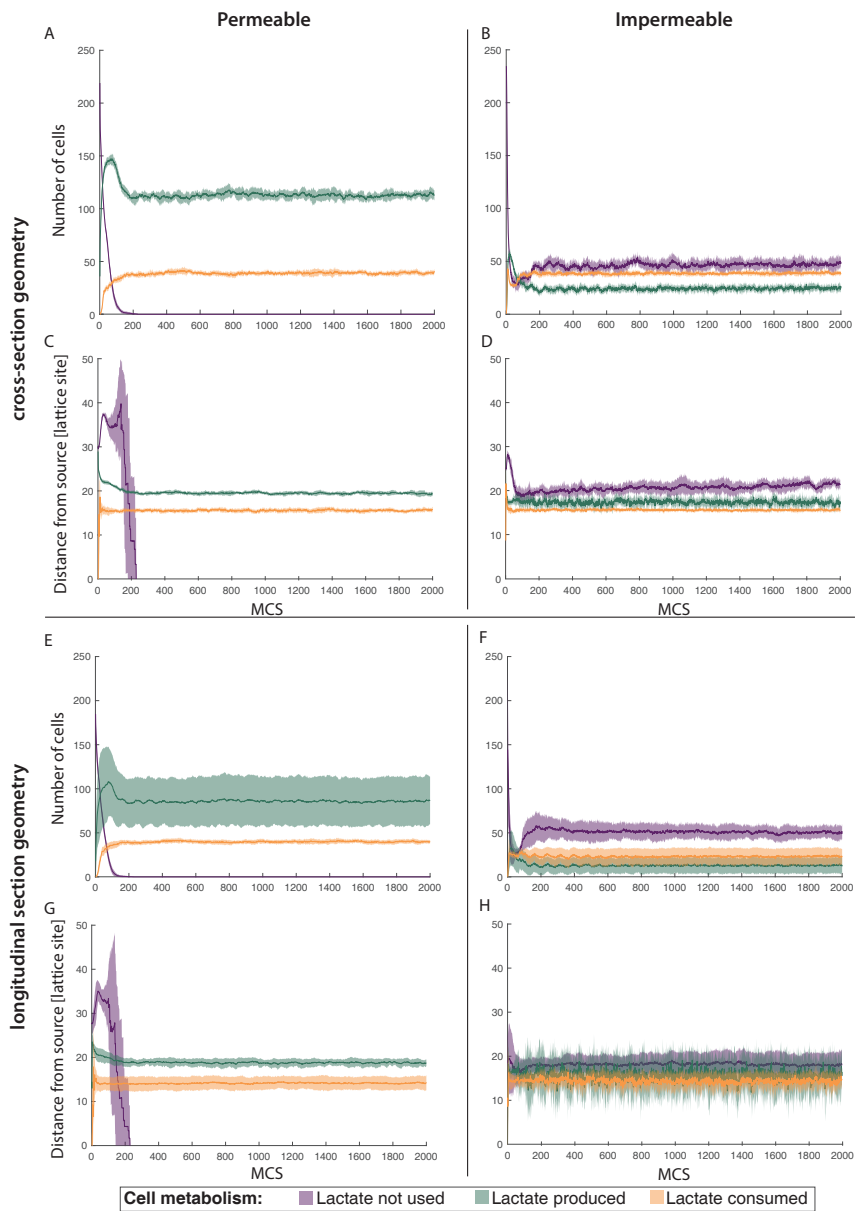


Figure 7. Comparison of the effect of cell permeability and simulation geometry on number and distance from source of cells of different metabolic phenotype. In panels A, B, C, D the geometry is shaped to represent a cross-section while in panels E, F, G, H it is shaped as a longitudinal section. Panels A, B, E and F depict the mean number of cells (solid line) and its standard deviation (shaded area) over 10 independent simulations. Panels C, D, G and H depict the mean distance of the cells from the closest nutrients source (solid line) and its standard deviation (shaded area) over 10 independent simulations, where the distance is calculated between the cell and the closest source barycentre. Biological cells are differently colored according the corresponding lactate metabolism, i.e. green if lactate is produced, orange is lactate is consumed and purple if lactate is both produced or consumed with a flux less than 0.1 fmol.

their metabolism: Outward lactate flux (green), Inward lactate flux (orange), No lactate flux (purple). Purple cells, corresponding to the ones that are not either consuming or producing lactate with a flux greater than 0.1 fmol, are missing among the permeable cells. These cells show a rapid drop in number in the early simulation cycles, completely disappearing at MCS 200, in both the cross-section (Figure 7 A to D) and longitudinal (Figure 7 E to H) simulation settings. The average number of lactate producing (outward flux, green) and their distance from the vessel was similar in both the cross-section and longitudinal simulations (panels A,B and E,F, respectively, of Figure 7), although the latter showed increased variability. In both cross- and longitudinal sections, lactate producing cells were present in higher number and farther to the vessels than lactate-consuming cells. Differently from permeable cells, the impermeable ones showed all the three types of lactate metabolism (Figure 6 and 7). Lactate producing (outward flux, green) cells represent the less abundant sub-population in both the longitudinal and cross-section simulation scenarios (panel B and F of Figure 7, respectively). Similar to the trend observed in permeable cells, longitudinal simulations of impermeable cells showed increased variability compared to cross-section variability (panels B, D and F, H of Figure 7), and a steady state was reached after about 200 MCS.

## 4. Discussion

In this work, we extended the previous FBCA methodology presented in [18, 23] to evaluate the impact of different nutrient diffusion models on the population dynamics. In particular, we modeled metabolic interaction among cells by allowing secreted metabolite to diffuse over the lattice together with the diffusion of nutrients from different sources.

We proved that the inclusion of the diffusion process in the system dynamics can characterize realistic and complex biological processes and phenomena. The developed simulator allowed to perform in depth quantitative analyses of cell populations properties in two different biological scenarios, namely a cell culture in a closed environment and a tissue. In the first scenario, the simulator faithfully reproduced the diauxic growth of yeast in a well stirred flask, whereas the second scenario properly mimicked the behaviour of a tissue organization or tumor micro-environment niche. In both cases, already known phenomena have been reproduced, such as for example the switch of the carbon source exploited to grow when the mainly used one is totally consumed.

In addition, our simulator showed the ability to discriminate cells having different ways of nutrient access according to their permeability, i.e. permeable and impermeable cells. Simulations regarding tissue experimental setting revealed that the corresponding geometry considerably influence cell positions within the lattice. Nevertheless, our model faithfully represented the cellular structure that we modelled like an *in vivo* cross or longitudinal sectioning of a biological tissue. This ability could be, in the future, exploited to model more complex and close to reality blood vessels configurations.

Overall, the choice of the most suitable experimental setting is linked to the aim of the research. A higher interest on the population dynamics rather than on the investigation of how nutrients are consumed by cells leads to consider permeable cells a better approximation. In the opposite case, impermeable cells result to be more appropriate.

In the next future we plan to perform further analyses to investigate the influence of different initial set of nutrients on cellular growth dynamics, as well as to explore any difference with the current

outcomes. This strategy could assist the analysis of the differences emerged in this work between alternative experimental settings. In particular, the reason why a more heterogeneous situation occurred only when impermeable cells were considered, could be investigated.

In view of the outcomes we obtained in this work, we are confident that our simulator is enough plastic to be adapted to the simulation of various and more complex scenarios, geometry of the system and nutrient diffusion process.

## References

- [1] Hanahan D, Weinberg R. Hallmarks of Cancer: The Next Generation. *Cell*, 2011. **144**:646–674. doi:10.1016/j.cell.2011.02.013.
- [2] Ward P, Thompson C. Metabolic Reprogramming: A Cancer Hallmark Even Warburg Did Not Anticipate. *Cancer Cell*, 2012. **21**:297–308. doi:10.1016/j.ccr.2012.02.014.
- [3] Orth JD, Thiele I, Palsson BØ. What is flux balance analysis? *Nature Biotechnology*, 2010. **28**:245. doi:10.1038/nbt.1614.
- [4] Cazzaniga P, Damiani C, Besozzi D, Colombo R, Nobile M, Gaglio D, Pescini D, Molinari S, Mauri G, Alberghina L, Vanoni M. Computational Strategies for a System-Level Understanding of Metabolism. *Metabolites*, 2014. **4**:1034–1087. doi:10.3390/metabo4041034.
- [5] Burrell RA, McGranahan N, Bartek J, Swanton C. The causes and consequences of genetic heterogeneity in cancer evolution. *Nature*, 2013. **501**:nature12625. doi:10.1038/nature12625.
- [6] Marusyk A, Almendro V, Polyak K. Intra-tumour heterogeneity: a looking glass for cancer? *Nature Reviews Cancer*, 2012. **12**:323. doi:10.1038/nrc3261.
- [7] McGranahan N, Swanton C. Biological and therapeutic impact of intratumor heterogeneity in cancer evolution. *Cancer cell*, 2015. **27**(1):15–26. doi:10.1016/j.ccell.2014.12.001.
- [8] Caravagna G, Graudenzi A, Ramazzotti D, Sanz-Pamplona R, Sano LD, Mauri G, Moreno V, Antoniotti M, Mishra B. Algorithmic methods to infer the evolutionary trajectories in cancer progression. *Proceedings of the National Academy of Sciences*, 2016. **113**:E4025–E4034. doi:10.1073/pnas.1520213113.
- [9] Lipinski KA, Barber LJ, Davies MN, Ashenden M, Sottoriva A, Gerlinger M. Cancer Evolution and the Limits of Predictability in Precision Cancer Medicine. *Trends in Cancer*, 2016. **2**:49–63. doi:10.1016/j.trecan.2015.11.003.
- [10] Navin NE. The first five years of single-cell cancer genomics and beyond. *Genome Research*, 2015. **25**:1499–1507. doi:10.1101/gr.191098.115.
- [11] Gawad C, Koh W, Quake SR. Single-cell genome sequencing: current state of the science. *Nature Reviews Genetics*, 2016. **17**:175–188. doi:10.1038/nrg.2015.16.
- [12] Cristini V, Lowengrub J. Multiscale modeling of cancer: an integrated experimental and mathematical modeling approach. Cambridge University Press, 2010. doi:10.1017/cbo9780511781452.
- [13] Deisboeck TS, Stamatakos GS. Multiscale cancer modeling. CRC Press, 2010. doi:10.1201/b10407.
- [14] Matteis GD, Graudenzi A, Antoniotti M. A review of spatial computational models for multi-cellular systems, with regard to intestinal crypts and colorectal cancer development. *Journal of Mathematical Biology*, 2013. **66**:1409–1462. doi:10.1007/s00285-012-0539-4.

- [15] Graudenzi A, Caravagna G, Matteis GD, Antoniotti M. Investigating the Relation between Stochastic Differentiation, Homeostasis and Clonal Expansion in Intestinal Crypts via Multiscale Modeling. *PLoS ONE*, 2014. **9**:e97272. doi:10.1371/journal.pone.0097272.
- [16] Rubinacci S, Graudenzi A, Caravagna G, Mauri G, Osborne J, Pitt-Francis J, Antoniotti M. CoGNaC: A Chaste Plugin for the Multiscale Simulation of Gene Regulatory Networks Driving the Spatial Dynamics of Tissues and Cancer. *Cancer Informatics*, 2015. **14**:53–65. doi:10.4137/cin.s19965.
- [17] Mina P, Bernardo Md, Savery NJ, Tsaneva-Atanasova K. Modelling emergence of oscillations in communicating bacteria: a structured approach from one to many cells. *Journal of the Royal Society, Interface*, 2013. **10**:20120612. doi:10.1098/rsif.2012.0612.
- [18] Graudenzi A, Maspero D, Damiani C. Modeling spatio-temporal dynamics of metabolic networks with cellular automata and constraint-based methods. In: Giancarlo Mauri ADKNLM Samira El Yacoubi (ed.), Cellular Automata. ACRI 2018. Lecture Notes in Computer Science, volume 11115. Springer, Cham, 2018 pp. 16–29. doi:10.1007/978-3-319-99813-8\_2.
- [19] Graner F, Glazier JA. Simulation of biological cell sorting using a two-dimensional extended Potts model. *Physical Review Letters*, 1992. **69**(13):2013–2016. doi:10.1103/physrevlett.69.2013.
- [20] Marée AF, Grieneisen VA, Hogeweg P. The Cellular Potts Model and biophysical properties of cells, tissues and morphogenesis. In: Single-cell-based models in biology and medicine, pp. 107–136. Springer, 2007. doi:10.1007/978-3-7643-8123-3\_5.
- [21] Scianna M, Preziosi L. Multiscale developments of the cellular Potts model. *Multiscale Modeling & Simulation*, 2012. **10**(2):342–382. doi:10.1137/100812951.
- [22] Szabó A, Merks RM. Cellular Potts Modeling of Tumor Growth, Tumor Invasion, and Tumor Evolution. *Frontiers in oncology*, 2013. **3**:87. doi:10.3389/fonc.2013.00087.
- [23] Maspero D, Graudenzi A, Singh S, Pescini D, Mauri G, Antoniotti M, Damiani C. Synchronization effects in a metabolism-driven model of multi-cellular system. volume 900. 2019 pp. 115–126. doi:10.1007/978-3-030-21733-4\_9.
- [24] Scianna M, Preziosi L. Cellular Potts Models: Multiscale Extensions and Biological Applications. CRC Press, 2013. doi:10.1201/b14075.
- [25] Filippo MD, Colombo R, Damiani C, Pescini D, Gaglio D, Vanoni M, Alberghina L, Mauri G. Zooming-in on cancer metabolic rewiring with tissue specific constraint-based models. *Computational Biology and Chemistry*, 2016. **62**:60–69. doi:10.1016/j.compbiolchem.2016.03.002.
- [26] Steinberg MS. On the mechanism of tissue reconstruction by dissociated cells, I. Population kinetics, differential adhesiveness, and the absence of directed migration. *Proceedings of the National Academy of Sciences*, 1962. **48**(9):1577–1582. doi:10.1073/pnas.48.9.1577.
- [27] Dan D, Mueller C, Chen K, Glazier JA. Solving the advection-diffusion equations in biological contexts using the cellular Potts model. *Physical Review E*, 2005. **72**(4):041909. doi:10.1103/physreve.72.041909.
- [28] Damiani C, Di Filippo M, Pescini D, Maspero D, Colombo R, Mauri G. popFBA: tackling intra-tumour heterogeneity with Flux Balance Analysis. *Bioinformatics*, 2017. **33**(14):i311–i318. doi:10.1093/bioinformatics/btx251.
- [29] Graudenzi A, Maspero D, Di Filippo M, Gnugnoli M, Isella C, Mauri G, Medico E, Antoniotti M, Damiani C. Integration of transcriptomic data and metabolic networks in cancer samples reveals highly significant prognostic power. *Journal of Biomedical Informatics*, 2018. **87**:37–149. doi:10.1016/j.jbi.2018.09.010.

- [30] Schellenberger J, Que R, Fleming RMT, Thiele I, Orth JD, Feist AM, Zielinski DC, Bordbar A, Lewis NE, Rahmanian S, Kang J, Hyduke DR, Palsson BØ. Quantitative prediction of cellular metabolism with constraint-based models: the COBRA Toolbox v2.0. *Nature protocols*, 2011. **6**(9):1290. doi: 10.1038/nprot.2011.308.